ChemComm

COMMUNICATION

View Article Online
View Journal | View Issue

Cite this: *Chem. Commun.*, 2015, 51, 2068

Received 25th November 2014,
Accepted 15th December 2014

DOI: 10.1039/c4cc09411e

www.rsc.org/chemcomm

Highly lithium-ion conductive battery separators from thermally rearranged polybenzoxazole†

Moon Joo Lee,‡[a] Ji Hoon Kim,‡[b] Hyung-Seok Lim,[a] So Young Lee,[b] Hyung Kyun Yu,[c] Jong Hun Kim,[c] Joo Sung Lee,[c] Yang-Kook Sun,[b] Michael D. Guiver,[bd] Kyung Do Suh*[a] and Young Moo Lee*[ab]

High power density lithium ion battery (HLIB) separators were fabricated for the first time from thermally rearranged poly(benzoxazole-*co*-imide) (TR-PBOI) nanofibrous membranes coated with TR-PBOI nanoparticles, which show distinct thermal and dimensional stabilities as well as excellent cycle retention and rate capability.

High energy density lithium ion batteries (LIBs) have recently been spotlighted and employed for electric vehicles (EV), power tools and energy storage systems (ESSs) as safety, reliability and durability of LIBs are required.[1–3] Commercially available polyolefin (PO) microporous membranes have been widely used as LIB separators due to their excellent mechanical strength, chemical and electrochemical stability. However, PO separators have material limitations such as inherently low affinity with electrolytes and they experience extensive shrinkage, particularly at high temperatures, which hinder their use in high capacity battery operation. For example, when a high capacity LIB is operating at 30 V_{DC}, which is considered a modest condition for EV or ESS, current passage through the PO separator results in an internal short and eventual explosion of the cell owing to enormous thermal shrinkage.[4–7]

Electrospun polymer membranes (ESMs) exhibit high porosity with reasonable mechanical strength even when they are very thin and are regarded as suitable for LIB applications. However, high mechanical strength of ESM is a critical requirement for practical use. Recently, many research groups have developed various ESMs and their composite membranes to enhance thermal and mechanical stabilities and reduce electrochemical resistance by increasing the affinity with the electrolyte and fabricating highly porous and thin membranes. For example, poly(butylene terephthalate) (PBT) ESM was tolerant up to 200 °C and showed similar discharge capacity and durability but it had lower ionic conductivity (0.27 mS cm^{-1}) compared with a commercial PO separator (0.47 mS cm^{-1}).[8] Polyimide (PI) ESM from the poly(amic acid) precursor showed stable discharge capacity and good cycle stability at the 0.2 C-rate as PI was stable up to 500 °C,[9] although the poly(amic acid) precursor was unstable at room temperature if stored for a long time. The poly(vinylidene fluoride) (PVDF) ESM exhibited good tensile strength (TS) (12 MPa) in both the machine direction (MD) and the transverse direction (TD) but elongation at break (EB) of the MD and the TD was quite different, 20% and 88%, respectively.[10] Too high an elongation at break at TD was an issue as ESM may contract in width. Inorganic particles such as SiO_2 were coated onto the polyethylene (PE) separator to achieve high thermal stability and dimensional stability, which increased the lithium ion conductivity to 0.79 mS cm^{-1}, 202% higher than the pristine PE separator.[11] Polyacrylonitrile (PAN)–SiO_2 composite ESM showed a very large pore size and pore size distribution (mean pore size = 0.49 μm and maximum pore size = 0.76 μm) and TS and EB of 23 MPa and 18%, respectively.[12] Inorganic composite membranes consisting of inorganic nanoparticles and PO or ESM have been developed due to their good thermal stability and capacity retention as potential LIB separators. On the other hand, ceramic coatings are inherently incompatible with polymer film, resulting in inconsistent current density and final battery failure due to local detachment of ceramic powders.[13]

Herein we describe for the first time novel copolymer membranes for high power density LIB separators; the so-called thermally rearranged poly(benzoxazole-*co*-imide) (TR-PBOI) electrospun membrane (P1) and the nanocomposite membrane with TR-PBOI particles (NCM, P2). Thermally rearranged polybenzoxazole (TR-PBO) has been first reported by us as a promising material for gas separation membranes due to its bimodal distribution of nanoporous cavities or free volume elements ranging from 0.3–0.4 nm and 0.8–0.9 nm cavities, which induce both extraordinary permeability and selectivity for small gas molecules as well as ions.[14–17] Due to its excellent thermal stability, chemical resistance

[a] *School of Chemical Engineering, College of Engineering, Hanyang University, Seoul 133-791, Korea. E-mail: kdsuh@hanyang.ac.kr*
[b] *Department of Energy Engineering, College of Engineering, Hanyang University, Seoul 133-791, Korea. E-mail: ymlee@hanyang.ac.kr*
[c] *Battery R&D, LG Chem., 104-1, Moonji-dong, Yuseong-gu, Daejeon, 305-380, Korea*
[d] *State Key Laboratory of Engines, School of Mechanical Engineering, Tianjin University, Tianjin, 300072, P. R. China*

† Electronic supplementary information (ESI) available: Synthesis, detailed experimental procedures and characterization data. See DOI: 10.1039/c4cc09411e

‡ Equally contributed to this work.

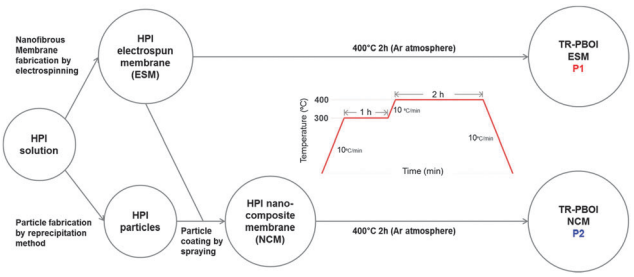

Scheme 1 Fabrication of the TR-PBOI electrospun membrane (P1) and the nano-composite membrane (P2) from the HPI copolymer.

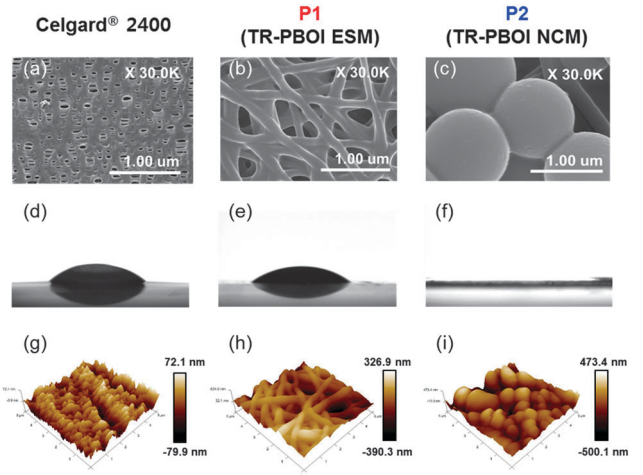

Fig. 1 Morphology of membranes was investigated by FE-SEM of (a) Celgard® 2400, (b) P1 and (c) P2 membranes. Wettability was determined by the contact angle test of (d) Celgard® 2400, (e) P1 and (f) P2 membranes after 0.5 s of the 1.15 M $LiPF_6$ electrolyte having fallen onto the membrane surface. Surface roughness of membranes was rendered by AFM of (g) Celgard® 2400, (h) P1 and (i) P2 membranes.

and good processability, it seems feasible to extend the scope to other applications. However, polyimides and polybenzoxazole particles have rarely been reported so far. While PBO particles have been described,[18] TR-PBOs have not been fabricated yet.

The procedure to fabricate the TR-PBOI copolymer ESM (P1) and the nanocomposite membrane (P2) is described in Scheme 1. We synthesized the hydroxypolyimide (HPI) copolymer as a precursor of TR-PBOI and prepared the ESM and nanoparticles using the HPI copolymer that were subsequently coated on top of the ESM having the same chemical composition as the nanoparticles (Sections S1–S4, ESI†). Then HPI nanoparticle coated ESMs (NCM) were converted into TR-PBOI composite membranes by thermal rearrangement reaction following the methods reported in our previous studies and as described in Section S5 (ESI†).[14,15,19] Here we report a novel TR-PBOI copolymer ESM (P1) and a NCM (P2) as potential candidates for an LIB separator that are compared with Celgard® 2400 as a reference in terms of electrochemical performance.

The HPI copolymer is synthesized from 4,4′-oxydiphthalic anhydride (ODPA), 3,3′-dihydroxy-4,4′-diamino-biphenyl (HAB) and 4,4′-oxydianiline (ODA) (Scheme S1, ESI†). The HPI copolymer prepared from 50 mol% HAB and 50 mol% ODA with dianhydride ODPA was denoted as ODPA-HAB_5-ODA_5. HPI copolymer membranes and nanoparticles were fabricated by the electrospinning and reprecipitation methods, respectively. The pristine HPI electrospun membrane and the HPI nanoparticle coated membrane underwent thermal treatment in a furnace under an argon atmosphere to convert them into TR-PBOI copolymer membranes. The experimental details are described in Sections S3–S5, ESI.†

The surface and cross-sectional structures of Celgard® 2400, P1 and P2 separators were verified using field emission scanning electron microscopy (FE-SEM) images (Fig. 1a–c, Fig. S2e, f, k and l, ESI†). Note that Celgard® 2400 (Fig. 1a) has a smaller pore size and more uniform pore structures compared with P1 and P2 (Fig. S4c, ESI†) and a composite membrane with nanoparticles was completely interconnected during thermal rearrangement without the need for polymer binders (Fig. S2f and l, ESI†). The change in chemical structure from HPI to TR-PBOI during thermal rearrangement was clarified by attenuated transmission reflection Fourier transform infrared (ATR-FTIR) spectroscopy (Fig. S3, ESI†). The wettability of separators to the electrolyte is regarded as one of the critical factors for low cost manufacturing and high electrochemical performance of a LIB. The wettability was evaluated by a contact angle analyser by dropping a non-aqueous liquid electrolyte which is 1.15 M $LiPF_6$ dissolved in ethylene carbonate (EC)/dimethyl carbonate (DEC) (7 : 3. v/v) onto the membrane surface, which shows the contact angle of each membrane at 0.5 s after dropping. The P2 membrane instantaneously absorbed the electrolyte, different from the wettability of P1 and Celgard® 2400 (Fig. 1d–f). Surface roughness, measured by atomic force microscopy (AFM) of the P2 membranes (Table 1 and Fig. 1g–i), was substantially enhanced after particle coating compared with uncoated P1. Both TR-PBOI membranes (P1 and P2) exhibited better wettability than Celgard® 2400 because of the presence of oxygen and nitrogen in the benzoxazole and imide structure of the copolymer.[20,21] The solubility parameter of the TR-PBOI copolymer membrane was calculated to be about 13 $(cal\ cm^{-3})^{1/2}$ whereas that of Celgard® 2400 was 16.5 $(cal\ cm^{-3})^{1/2}$, while the electrolyte showed 10.6 $(cal\ cm^{-3})^{1/2}$ according to the Hildebrand method.[22,23] Therefore TR-PBOI exhibited inherently higher compatibility with a liquid electrolyte than Celgard® 2400. Both P1 and P2 also possessed significantly higher porosity (62%) and electrolyte uptake (>88%) than Celgard® 2400 (41% and 61%) (Table 1). The benefits of high wettability are reduced time and energy for assembly of LIB cells. Moreover, compatibility between the separators and electrolyte reduces the overall cell resistance and thus leads to increased ionic conductivity of the cell. Physical and surface properties of these membranes are summarized in Table 1.

The superior thermal stability of P1 and P2 compared with Celgard® 2400 is shown by thermogravimetric analysis (TGA) and differential scanning calorimetry (DSC). As can be seen in Fig. 2a, both P1 and P2 membranes showed no weight loss until degradation occurred at 600 °C while the Celgard® 2400 decomposed below 400 °C. DSC curves show that the Celgard® 2400 separator has a melting point at around 160 °C while the TR-PBOI membranes showed no melting peaks up to 400 °C (Fig. 2b). In addition, thermal shrinkage of separators was identified by measuring the dimensional stability of separators at 170 °C (Fig. 2c). Note that P1

Table 1 Porosity, surface properties and lithium ion conductivities of membranes used in this research

	Celgard® 2400	P1	P2
Composition	PP	TR-PBOI	TR-PBOI
Thickness [μm]	25 ± 1	30 ± 5	49 ± 7
Tensile strength [MPa] (MD[a]/TD[b])	168 ± 10.7/11 ± 4.7	39 ± 0.2/38 ± 0.6	29 ± 0.4/18 ± 2.5
Elongation [%] (MD[a]/TD[b])	33 ± 0.9/315 ± 20.4	40 ± 3.0/31 ± 0.7	32 ± 0.4/21 ± 8.1
Mean pore size [μm]	0.03 ± 0.003	0.26 ± 0.05	0.15 ± 0.03
Porosity [%]	41 ± 1.24	62 ± 0.71	62 ± 1.52
Contact angle [°]	41 ± 3.08	35 ± 1.75	N/A
Electrolyte uptake [%]	61 ± 3.7	88 ± 5.8	110 ± 4.9
Surface roughness [nm]	14 ± 0.4	70 ± 14.6	130 ± 34.1
Solubility parameter $[(\text{cal cm}^{-3})^{1/2}]$[22]	16.5	13.0	13.0
Li^+ conductivity $[10^{-3}\ \text{S cm}^{-1}]$	0.473	1.11	1.50

[a] Machine direction (MD). [b] Transverse direction (TD); all the characterization methods are described in Section S6, ESI.

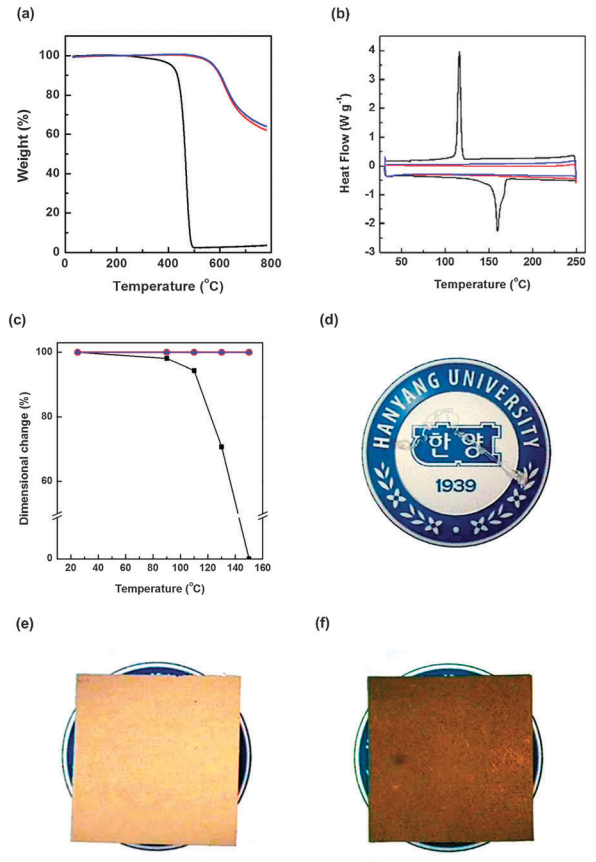

Fig. 2 Thermal stability of membranes (— Celgard® 2400, — P1 and — P2). (a) TGA curves of three membranes show that Celgard® 2400 decomposes starting from 400 °C whereas P1 and P2 prolong their decomposition above 600 °C. Note that TR-PBO nanocomposite membrane P2 has a char yield of over 50% above 800 °C. (b) DSC scan curves of P1 and P2 compared with reference material Celgard® 2400, P1 and P2 do not show any melting up to 250 °C whereas the Celgard® 2400 exhibits melting at 160 °C. (c) Thermal shrinkage of membranes (—■— Celgard® 2400, —●— P1 and —▲— P2) was determined by investigating the dimensional change of membranes at 90, 110, 130 and 150 °C for 1 h, consecutively. The surface images of (d) Celgard® 2400, (e) P1, and (f) P2 were observed after completing the thermal shrinkage test.

and P2 showed no dimensional changes during heating, unlike Celgard® 2400 (Fig. 2d–f).

Mechanical properties of P1, P2 and Celgard® 2400 were evaluated following ASTM 638-5 (Fig. S4, ESI†). P1 shows uniform mechanical properties in both directions (MD and TD) and has the highest tensile strength compared with reported nascent electrospun membranes.[9,10,12] However, compared with P1, the tensile strength and elongation at break of P2 decreased from 39 ± 0.2 MPa of TS and 40 ± 0.6% of EB to 29 ± 0.4 MPA and 32 ± 0.4% in MD and also decreased from 38 ± 0.6 MPa of TS and 40 ± 3.0% of EB to 18 ± 2.5 MPa and 21 ± 8.1% in TD, respectively. If the P2 membrane is stretched, the particle coating layer could be easily damaged due to weak interconnection between particles. Since the damaged part of the particle layer expedites the membrane to break, the P2 membrane shows lower tensile strength and elongation at break than the pristine TR electrospun membrane (P1). Although Celgard® 2400 shows excellent tensile strength and elongation at break (168 ± 10.7 MPa and 33 ± 0.9%, respectively) in MD, the tensile strength of TD is too low (11 MPa). Therefore, dimensional stability of Celgard® 2400 is low particularly in TD. However, P1 and P2 membranes have sufficient mechanical strength (>30 MPa) to withstand mechanical handling and excellent thermal and dimensional stability (>400 °C) as well as small and narrow pore size distribution (<0.26 nm ± 0.05, Fig. S4, ESI†) suitable for LIB application.

The electrochemical stability windows of P1 and P2 were checked by linear sweep voltammetry (LSV, VMP3, Bio-Logic, France). In Fig. S5 (ESI†), the current flows of P1 and P2 were very small when the voltage was below 5.0 V (*vs.* Li/Li^+), indicating that no decomposition of the polymer and the electrolyte occurs below this potential. Other experimental details are described in Section S7, ESI.†

The electrochemical impedance spectra of the three separators are illustrated as Nyquist plots in Fig. 3a. Each separator was sandwiched between stainless steel plates, soaked by 1.15 M $LiPF_6$ which was dissolved in EC/DEC (3/7, v/v) and packaged in a pouch cell and operated at 25 °C. The P2 separator had the lowest resistance among the three separators (47% lower than the Celgard® 2400). The resistance of the P1 separator was also much lower (40%) than that of Celgard® 2400. Surprisingly, the ionic conductivities of P2 and P1 exhibited values of more than three-fold and two-fold that of the Celgard® 2400 (Table 1). Nonetheless, the resistance of P1 and P2 was significantly diminished (about 53% and 60%) compared with that of Celgard® 2400. Due to the excellent electrolyte wettability of the TR-PBOI copolymer membranes, the bulk resistance of the

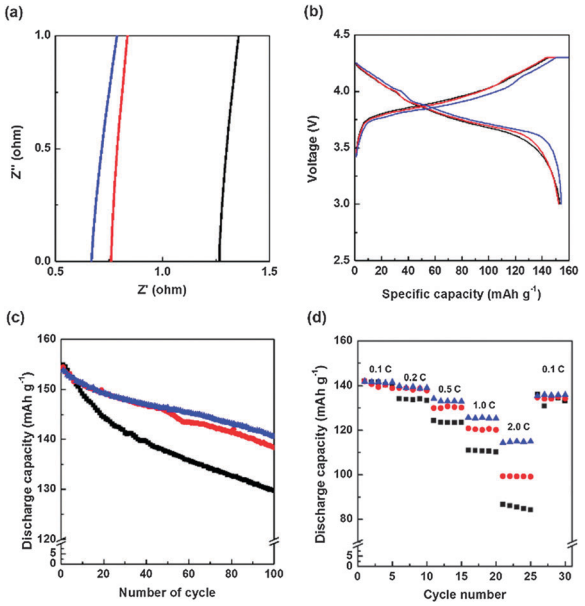

Fig. 3 Electrochemical performance of separators (Celgard® 2400 (-), P1 (---) and P2 (---)). (a) Nyquist plot of AC impedance spectra of the separators. (b) The charge-discharge profile of the separators at the 1st cycle. (c) The cycle retention of cells (Celgard® 2400 (■), P1 (●) and P2 (▲)) consisting of the separators, $LiCoO_2$, graphite and 1.15 M $LiPF_6$ in EC:DEC (3 : 7, v/v%) under a voltage range of 3.0–4.2 V at the 0.5 C-rate. (d) The rate capability was tested at 0.1, 0.2, 0.5, 1.0 and 2.0 C-rates for the cells.

membrane decreased substantially, thus facilitating the transportation of lithium ions across the separator.

Coin-type full-cells (CR 2032) were employed for electrochemical measurements. Natural graphite (Welcos, Japan) and $LiCoO_2$ (LCO, Welcos, Japan) were used as the anode and the cathode, respectively. In addition, 1.15 M $LiPF_6$ in EC : DEC (3 : 7, v/v%, Techno Semichem Co. Ltd., Korea) was applied for the liquid electrolyte. Other details for the electrochemical test are described in Section S7, ESI.† The initial charge–discharge curve of the cells using the Celgard® 2400, P1 and P2 (Fig. 3b) indicates the resistance induced by the separator. Because the other parts of the cell are the identical for the separator, the first cycle profile of P2 exhibits lower ohmic and concentration polarization loss than that of P1 and Celgard® 2400.

The cycle retention of the cells using the Celgard® 2400, P1, and P2 was investigated as shown in Fig. 3c at a charge–discharge rate of 0.5 C-rate at 25 °C. The cycle retention of the cell incorporating P2 maintained stable behavior during 100 cycles; the initial and final discharge capacity was 154.4 mA h g^{-1} and 140.8 mA h g^{-1}, respectively, with a total capacity loss of 9%. The P1 showed competitive performance compared with the P2, with 10% loss from the initial discharge capacity, whereas Celgard® 2400 had up to 16% loss. The prolonged cycling performance of the TR-PBOI copolymer separators could be attributed to outstanding thermal stability and electrochemical stability as well as the beneficial wettability and low cell resistance.

The rate capability test was also investigated for the cells composed of Celgard® 2400, P1 and P2 from the0.1 to 2 C-rate as shown in Fig. 3d. At a high C-rate, the lithium ion conductivity had a significant effect on cell performance. For that reason, all the cells gradually lost their discharge capacity depending on the C-rate. At the 2.0 C-rate, Celgard® 2400 exhibited a 40% loss of total discharge capacity while P1 and P2 showed a more stable rate capability with 30% and 20% losses, respectively, against total discharge capacity. Note that high C-rate performance is essential for fast-charging LIBs of electric vehicles. This result suggests that P1 and P2 TR copolymer membranes are potentially much better battery separators due to their high porosity, interconnected pore structure and excellent electrolyte wettability.

In conclusion, we successfully developed for the first time TR-PBOI ESM (P1) and NCM (P2) LIB separators showing excellent thermal and dimensional stability and low cell resistance. P2 showed superior performances to P1 due to the fact that the nanoparticle coating layer improved wettability to the electrolyte, decreased electrolyte resistance and facilitated the ion conductivity. However, all the TR-PBOI copolymer membranes displayed better cycle retention and rate capability compared to the commercial separators, demonstrating that the TR-PBOI copolymer composite membranes are excellent candidates for high capacity LIB separators.

The authors acknowledge the financial support of the Nano Materials Technology Development Program, National Research Foundation (NRF) of the Korean Ministry of ICT, Science and Technology (2012M3A7B4049745) and partial support from LG Chem. Co. Ltd.

Notes and references

1 S. Cavaliere, S. Subianto, I. Savych, D. J. Jones and J. Rozière, *Energy Environ. Sci.*, 2011, **4**, 4761.
2 J. Hassoun, S. Panero, P. Reale and B. Scrosati, *Adv. Mater.*, 2009, **21**, 4807.
3 H. Lee, M. Yanilmaz, O. Toprakci, K. Fu and X. Zhang, *Energy Environ. Sci.*, 2014, **7**, 3857.
4 S. Jayaraman, V. Aravindan, P. Suresh Kumar, W. C. Ling, S. Ramakrishna and S. Madhavi, *Chem. Commun.*, 2013, **49**, 6677.
5 H. Jia, J. Wang, F. Lin, C. W. Monroe, J. Yang and Y. NuLi, *Chem. Commun.*, 2014, **50**, 7011.
6 M. H. Ryou, Y. M. Lee, J. K. Park and J. W. Choi, *Adv. Mater.*, 2011, **23**, 3066.
7 J. Shi, H. Hu, Y. Xia, Y. Liu and Z. Liu, *J. Mater. Chem. A*, 2014, **2**, 9134.
8 C. J. Orendorff, T. N. Lambert, C. A. Chavez, M. Bencomo and K. R. Fenton, *Adv. Energy Mater.*, 2013, **3**, 314.
9 Y. E. Miao, G. N. Zhu, H. Q. Hou, Y. Y. Xia and T. X. Liu, *J. Power Sources*, 2013, **226**, 82.
10 M. Tian, C. Q. Qiu, Y. Liao, S. R. Chou and R. Wang, *Sep. Purif. Technol.*, 2013, **118**, 727.
11 W. K. Shin and D. W. Kim, *J. Power Sources*, 2013, **226**, 54.
12 X. X. Song, Z. Y. Liu and D. D. Sun, *Energy Environ. Sci.*, 2013, **6**, 1199.
13 X. Huang, D. Bahroloomi and X. Xiao, *J. Solid State Electrochem.*, 2013, **18**, 133.
14 S. H. Han, N. Misdan, S. Kim, C. M. Doherty, A. J. Hill and Y. M. Lee, *Macromolecules*, 2010, **43**, 7657.
15 C. H. Jung, J. E. Lee, S. H. Han, H. B. Park and Y. M. Lee, *J. Membr. Sci.*, 2010, **350**, 301.
16 S. Kim, S. H. Han and Y. M. Lee, *J. Membr. Sci.*, 2012, **403**, 169.
17 H. B. Park, C. H. Jung, Y. M. Lee, A. J. Hill, S. J. Pas, S. T. Mudie, E. Van Wagner, B. D. Freeman and D. J. Cookson, *Science*, 2007, **318**, 254.
18 Y. Yoshioka, *Open Surf. Sci. J.*, 2012, **4**, 1.
19 M. Calle, A. E. Lozano and Y. M. Lee, *Eur. Polym. J.*, 2012, **48**, 1313.
20 A. B. D. Cassie and S. Baxter, *Trans. Faraday Soc.*, 1944, **40**, 546.
21 A. Tuteja, W. Choi, M. Ma, J. M. Mabry, S. A. Mazzella, G. C. Rutledge, G. H. McKinley and R. E. Cohen, *Science*, 2007, **318**, 1618.
22 A. F. M. Barton, *CRC Handbook of Solubility Parameters and Other Cohesion Parameters*, Taylor & Francis, 2nd edn, 1991.
23 R. F. Fedors, *Polym. Eng. Sci.*, 1974, **14**, 147.